International Journal of Engineering Trends and Technology
ISSN: 2231–5381 / https://doi.org/10.14445/22315381/IJETT-V73I11P122

Volume 73 Issue 11, 312-324, November 2025

Original Article

Development of Multi-Band Sub-6 GHz MIMO Antenna Using Complementary Split Ring Resonator and Defected Ground Structure

Basavaraju D R[1], Sukumar Ramanujam[2]

[1,2] *FET, JAIN (Deemed to be University), India.*

[1]*Corresponding Author : dr.basavaraju@jainuniversity.ac.in*

Received:08 August 2025 Revised: 05 November 2025 Accepted: 15 November 2025 Published: 25 November 2025

Abstract - *This study presents a multi-band, two-port MIMO antenna incorporating a Complementary Split Ring Resonator (CSRR) on the radiating patch and an inverted-L shaped slot on the ground plane. The design is tailored to support WiMAX, 5GHz Wi-Fi, and Advanced 5G Applications. The proposed MIMO antenna works at three frequency bands centered at 3.6 GHz, 4.47 GHz, and 5.53 GHz. The optimized circular CSRR with diagonal splits introduced on the radiating patch yields one more resonance frequency band by converting a wideband to a dual-band antenna. The Square loop structured strip line, Coplanar Waveguide (CPW) feed, improves the bandwidth and impedance matching. An inverted-L-shaped slot on the ground plane generates a multi-band characteristic by introducing one more band from 5.16 GHz to 7 GHz. The designed antenna has a dimension of 63 x 20 x 1.6 mm3. The FR4 substrate with a dielectric constant of 4.4, a thickness of 1.6 mm, was used for the simulation as well as fabrication. The implemented antenna is examined with MIMO performance parameters, and simulated and measured quantities are in good agreement. The Simulated results of S21 less than -24dB, ECC<0.0035, DG>9.999 dB, TARC less than -10dB, and CCL < 0.175 bits/sec/Hz for all three bands were obtained. The overall gain of the MIMO was found to be 3.1dBi. The analysis shows that the incorporation of CSRR resulted in a dual-band with slightly improved gain, and the CPW feed improves the gain as well as the bandwidth. The defective ground structure (inverted-L -L shape) leads to the multi-band characteristic. The antenna was fabricated, and its performance was tested with a Vector Network Analyzer (VNA). The results signify that the implemented antenna is a potential candidate for applications in the 5G Sub-6 GHz Band.*

Keywords - *MIMO, CSRR, DGS, Sub-6 GHz.*

1. Introduction

The rapid technological evolution, particularly in fifth-generation wireless communications, has increased the demand for high-performance antenna systems. The Sub-6GHz band of 5G contributes significantly to wireless communication. Sub 6-GHz ensures widespread and reliable connectivity compared to the millimetre wave, which offers high speed with limited range. To efficiently use the sub-6 GHz spectrum, an antenna with multiple elements that supports multi-band as well as stable performance parameters is required. The ability of the MIMO antennas to enhance channel capacity and reduce multipath fading without additional power and bandwidth has gained attention. Conventional methods, such as parasitic elements, slots, and stubs, will increase the antenna size or limit control on frequency tuning. To meet the day-to-day user demands for higher data rates, reliability, and proper spectrum utilization, metamaterial-based MIMO antennas play a critical role in today's research. Use of metamaterials with the MIMO antennas further enhances the performance, such as gain, bandwidth, isolation, miniaturisation, etc, due to their material properties. These are artificially structured materials having negative permittivity and permeability that affect the propagation of electromagnetic waves. Split Ring Resonators (SRRs) and CSRRs play a prominent part in the design of high-performance, miniaturised MIMO antennas. SRRs are basically a metallic ring with a split, whereas CSRRs are two metallic rings with a gap in the opposite faces that creates a resonance at a particular frequency. The SRRs manipulate the magnetic field to modify the propagation, whereas CSRRs manipulate the electric field. The Coplanar Waveguide (CPW) feed has a great research interest due to its ability to reduce the coupling, providing better impedance matching and ease of fabrication in the field of MIMO antennas. Multiple patterns of DGS play a vital role in suppressing surface wave propagation and minimizing coupling. This leads to increased isolation and diversity performance of MIMO, which is essential for reliable communication. Miniaturisation, impedance matching, and bandwidth characteristics can also be enhanced with specific patterned DGS. However, the

design of multiple resonance antennas over a small form factor needs a trade-off among performance parameters. Hence, research on MIMO with DGS has received more attention in today's 5G era.

A symmetrically X-shaped two-port MIMO antenna was designed, and the design process consists of four stages: design of rectangular MSPA, etching a slot, adding a stub, and making the structure X-shaped to meet the requirement. The meta surface structure was positioned on the radiating elements, which increased the gain as well as isolation between the elements, and also achieved circular polarisation. The antenna resonates at 3.27 GHz and 4.78 GHz [1]. An antenna with a CSRR at the ground plane was introduced, which operates at two mm-wave frequency bands. The CSRR on the ground yields a frequency shift as well as a wider bandwidth. The design does not need additional structure for decoupling, since the values are above 15 dB [2]. A metamaterial-based CPW-fed MIMO antenna implemented using a hexagonal open ring resonator and split ring resonators. The antenna works at two bands in sub-6 GHz, the lower band (3.78-2.8 GHz) resulted due to the hexagonal ring resonators, whereas the higher band (6.38-5.38 GHz) was achieved with the Split ring resonators. The isolation of -25dB, gain of 5dBi, and efficiency of 97% were achieved with the antenna dimensions 47.4*31.7*1.6 mm3 [3]. A pentagonal-shaped two-element MIMO antenna with circular slots on the radiators has been designed to improve the isolation and gain. The rectangular-shaped stub improved the bandwidth. Use of low εr and thicker substrates is preferred for UWB [4]. The 4-element high isolation, low substrate loss MIMO antenna has been designed. Each element contains 3 × 3 resonating elements with matching stubs. The DGS and Dielectric slots were incorporated to improve the isolation among radiating elements. Performance was improved by reducing the effect of surface wave propagation and loss of substrate [5].

The reconfigurable MIMO antenna with PIN diodes and DC biasing networks was implemented. The PIFA antenna structured antennas operate in multiple bands covering LTE, GSM, UMTS, and 5G-NR bands. BAR50-02V PIN diode used as a switch to each antenna to achieve reconfigurability in frequency and radiation pattern [6]. The corner truncated patch with partial ground, including a half-circle SRR and stub over a feed line, is included. Machine learning was employed to find the best position and dimensions of the parasitic elements, ground plane for the MIMO operating in the sub-6 GHz frequency band [7]. Radiators tilted clockwise by 45 degrees, incorporated slots that yield high isolation via current path enhancement. Results are satisfactory with the measurements. [8]. A microstrip antenna with a superstrate material and reconfigurability using a varactor diode is achieved. Superstrate is of circular and hexagonal shapes, which boost performance. The diodes incorporate reconfigurability along with the superstrates [9]. Circular patches with defective ground and slots are placed orthogonally to form a MIMO that operates at three frequency bands with an improved isolation of 30dB. The isolation between the radiating elements was achieved through orthogonal placements, and a triple-band response was obtained through defected ground structures and slots. Defected grounds were tapered at the edges to obtain the impedance matching [10].

The patches are formed in the form of a half-moon, and slots are employed at the ground to achieve wideband, multi-band characteristics. The ground slots convert the band from narrow to wide with gain improvement. The optimum results were obtained by varying the dimensions of the slot and the position of the feed [11]. A two-port MIMO having wide slots between radiating elements has been proposed to obtain high isolation, and open-ended slots were introduced to yield multiple operating bands. Stepped impedance feed is used on the top and meander lines with slots at ground [12]. U-shaped meander line structure is used with the radiating patches to improve the decoupling between antenna elements. The designed structure operates at two frequency bands with a gain of 7.35dBi and an isolation of -27dB. The meander line feed structures resulted in the differential phase shift at the ports [13]. The bandwidth and impedance matching were obtained by incorporating elliptical monopole and square-shaped parasitic elements with the antenna. The isolation achieved with the introduction of the slit in the ground [14]. A multi-band ability for the MIMO antennas was achieved through the spider-shaped fractal on the patch, and the ground plane was etched in the form of Y structures connected to DGS, which improves the isolation among the elements [15].

The MIMO with two monopole antennas placed orthogonally to achieve better isolation has been presented. Polarization diversity was achieved through orthogonal placement. Half ground plane, metal strips connected act as stubs, improving the decoupling [16]. MIMO antenna designed with two monopole open loop resonators. The complementary resonators result in resonance at one band, whereas slots on the feedline, along with stepped stubs, yield two more bands [17]. The multi-band MIMO antenna is designed by inserting a slot, an inverted-L, and an ohm symbol. The antenna operates at five different frequency bands. Inverted-L and ohm symbol resulted in the improvement [18].

The design consists of two closely spaced, radiating elements that form a MIMO antenna. Mutual coupling was reduced by placing a square-shaped split-ring resonator over antenna elements. The meta surface SRRs act as a medium with negative permeability [19]. A two-element MIMO consisting of a triangular patch with slits and a frequency-selective surface in the middle of the antenna, designed for multi-band operations. Slits on the patch improved the bandwidth, and a thin strip results in impedance matching

[20]. A multi-band MIMO antenna designed with two symmetrically placed patch elements fed with CPW. The neutralising line is used to nullify the reactive coupling, whereas four slits were etched to improve the mutual coupling and impedance matching [21]. Microstrip antenna loaded with CSRR operating at three frequency bands. Multi-band obtained through CSRR, whereas higher modes are suppressed via plated holes. Design provides beam steering till 80 degrees [22]. The microstrip patch performance has been evaluated by placing a single octagonal CSRR and multiple OCSRRs. The patch with multiple OCSRR shows the improvement in the bandwidth by 60MHz compared to a single OCSRR [23]. A square microstrip patch antenna equipped with CSRR structure has been designed to achieve a dual-band operation. The higher band was obtained through the patch, whereas the lower band was achieved by the incorporation of CSRR [24]. A semicircular monopole antenna, along with C-shaped slots, was proposed in this paper.

The structure was also loaded with the CSRR. CSRR slots on the ground plane introduced a frequency band for WiMAX (3.73 GHz), whereas quarter wavelength slots yield two more bands for GSM (1.77 GHz) and C-Band (4.15 GHz) [25]. Traditional patch antenna performance has been compared and analysed with an antenna loaded with CSRR (VSWR, Gain, Bandwidth, and Size). Also, the bending effect of the antenna has been analysed [26]. Multi-band operation is achieved by introducing CSRR on the ground. A miniaturised square patch antenna is designed by placing a CSRR structure between the radiator and the ground. The comparison results show a better improvement in the efficiency, bandwidth, and area with respect to the traditional square patch antenna [27, 28].

An antenna with a dual hook shape implemented for the applications of Wi-Fi 6E and 5G operating at 7.1 GHz, 3.6 GHz over FR4 dielectric material. Efficiency and impedance matching were improved by the application of a parasitic element along with DGS. The antenna with a compact size of 19 *36 mm2 produces a bandwidth of 10.21% and 14.08% respectively. Achieved peak gain of 3.85 dBi and isolation above -29 dB, -21 dB [29]. Dual and multi-band MIMO designed using the principle of microstrip line for below 6 GHz 5G applications. Inverted-L slots were used to achieve a multi-band operation over a small footprint. The initial design has a broadband characteristic from 4.30 to 5.54 GHz that was converted to dual band with the application of slots. One more inverted-L at the opposite side yields a triple band covering frequencies 3.725 GHz, 4.9 GHz, and 6.4 GHz. Gain of 5dBi, CCL < 0.5 bits/sec/Hz, ECC (<0.02), and isolation of -23dB were achieved [30]. Compact and dual-band behaviour of the flexible MIMO antenna was achieved through the modification of a rectangular radiator with a dual L-shaped strip and a minimized ground plane. The antenna has a footprint of 57*50 mm2 covering 3.7 GHz and 5.8 GHz with the gains of 5.2dBi and 7.7 dBi. Isolation (>22 dB) was achieved through DGS. Moreover, the antenna exhibits low SAR values that demonstrate its ability for wearable as well as compact 5G devices [31]. The purpose of this research work is to implement a multi-band MIMO antenna operating below Sub-6 GHz to cover WiMAX, 5GHz Wi-fi, and Advanced 5G applications using a metamaterial CSRR structure on the radiating patch. The structure of the paper has the following sections: The need for MIMO, employing Metamaterial structures on the antennas, and CPW feed in 5G Wireless communication is covered in the Introduction in Section 1. Section 2 discusses the antenna geometry, dimensions, and its evolution. Stage 3 provides the stagewise improvement in the performance parameters. The simulated results and discussion of MIMO performance parameters are presented in Section 4. The fabrication of the designed antenna and its performance comparison are in Section 5. Practical implications of the fabricated antenna are mentioned in Section 6, and the conclusion is in Section 7.

2. Antenna Design and Its Evolution

Initially, the single square Micro-Strip Patch Antenna (MSPA) was designed using a FR4 substrate (εr=4.4), a thickness of 1.6mm, and a tangent loss of 0.02. The performance parameters were analysed through the HFSS simulator with adaptive convergence (Δs) equal to 0.01 and a discrete sweep starting at 1 GHz to 7 GHz. The goal of this research is to develop a multi-band MIMO antenna for 5G Sub-6 GHz applications. To achieve that, the narrowband patch is converted to a wideband antenna by introducing a partial ground plane. The partial ground improves the bandwidth by increasing the fringing fields around the patch edges. The partial ground resulted in the wideband operation from 3.47 GHz to 6.02 GHz with a centre frequency of 4.58GHz.

To introduce one more band, a metamaterial CSRR structure is etched in the middle of the radiating patch. CSRR on the radiating patch creates a resonance at 3.8 GHz by disturbing the current distribution. The resonant frequency of the CSRR structure is governed by Equation (1). The dimensions of inner, outer radius (R1 and R2), εr, substrate height (h), and the split gap (g) majorly decide the resonance of the presented CSRR structure with negative permittivity.

The CSRR illustrates a notch-band characteristic in the wider bandwidth and creates two bands. The square loop strip line structure is added at the patch's top right corner. The parasitic effect of the square loop strip structure is utilized to tune the antenna's bandwidth and return loss. CSRR patch antenna gives a dual-band with centre frequency of 3.8 GHz and 4.9 GHz. It is noticed that the introduction of the CSRR yields an improvement in the gain from 2.5 dBi to 2.66 dBi. The CPW feed is introduced to the CSRR-loaded patch to enhance impedance matching. The dimensions and performance parameters of the partial ground antenna, CSRR-

loaded antenna, CPW-fed CSRR-loaded antenna, and MIMO are presented in Table 1.

$$f_{NB-SRR} = \frac{c}{2\pi^2}\sqrt{\frac{3(R1-R2-W)}{Re(\varepsilon_r)R_1^3}} \quad (1)$$

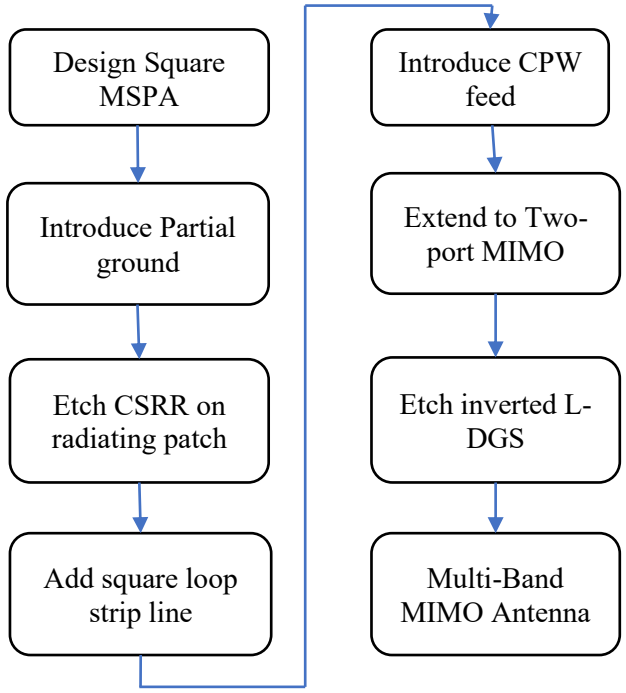

Fig. 1 Workflow of the proposed multi-band MIMO antenna

A single element is extended to form a two-port MIMO, and an inverted-L shaped defected ground structure is introduced to get multi-band operation from the dual-band. The Square loop strip line structures were tuned to get better antenna characteristics. The proposed two-port MIMO operates at multiple bands with resonant frequencies of 3.6 GHz, 4.47 GHz, and 5.53 GHz. A flow diagram of the proposed antenna is presented in Figure 1. Figure 2 shows the step-by-step evolution of the MIMO antenna.

3. Performance Analysis of the Proposed Antenna Stage by Stage

The antenna is designed by going through the following four stages.

Stage 1: Square microstrip Patch antenna design and introducing partial ground.

The initial square MSPA was resulting in a narrowband operation. To increase the bandwidth, the ground plane dimension was reduced to 34.3% as in Figure 2(a). The partial ground modifies the confined surface current in the full ground and results in a wider bandwidth of 2.55 GHz (3.47 GHz - 6.02 GHz) with good return loss of -34.66 dB, as tabulated in Table 1. The antenna gain with partial ground is around 2.5 dBi. The impedance value of 1.0194 + 0.0319i ohms indicates excellent impedance matching.

Stage 2: CSRR structure etched in the middle of the radiating patch, and adding a square loop strip line.

The non-biaisotropic complementary split ring resonator (NB-SRR) structure etched on the centre of the radiator [3] as shown in Figure 2(b). The SRRs are placed with gaps on the opposite side, breaking the symmetry and making the resonator deal with the magnetic field. The inner radius (R1), Outer radius (R2), and the gap (g) were tuned manually to gain the resonance at 3.89 GHz. The value of g is chosen in such a way as to increase the capacitive coupling and to decrease the frequency of resonance. The value of g also decides the notch band characteristics of the CSRR structure, thereby allowing for filtering out of the selective band. The optimised values of R1, R2, and g are found to be 2.22 mm, 4.285 mm, and 0.78 mm, as in Table 1. Also, it can be observed that the introduction of CSRR results in converting a wideband antenna to a band (resonances at 3.89 GHz and 4.9 GHz) antenna. The slight shift in the resonance frequency of stage 1 can be observed from 4.58 GHz to 4.9 GHz with a slight increase in the gain of 0.16 dB due to its metamaterial property. A square loop strip line with a width of 0.2 mm and a total length of 7.2 mm is used to tune the bandwidth and impedance matching. Return loss values are found to be -28.25 dB, -22.71 dB, with a bandwidth of 3.08 GHz-4.48 GHz (1.4 GHz) and 4.69 GHz- 6.54 GHz (1.85 GHz).

Stage 3: Incorporating CPW feed

The incorporation of the CPW feed with the CSRR structure shows enhancement in return loss and a slight shift from 3.89 GHz to 4.1 GHz in the first band, whereas from 4.9 GHz to 5 GHz in the second band.

The CPW feed also resulted in a wider bandwidth in the higher resonance frequency (4.13 GHz), as indicated in Table 1. The impedance values (0.9982 + 0.0169i) at f1 and (1.1313 + 0.1290i) at f2 indicate an extremely good match at band 1 and a slight mismatch at band 2 due to parasitic effects. The CPW ground width (Wcpw), spacing between feed line and CPW ground (s), controls the characteristic impedance, and the length of the CPW ground (Lcpw) impacts the resonances' behaviour. The careful tuning of Lcpw, Wcpw, and S controls impedance matching (return loss), bandwidth, and radiation patterns. Figure 2(c) presents the CPW feed on the antenna. The variations of S11, gain, and VSWR in the first three stages of the antenna are shown in Figures 3 and 4.

Stage 4: Extend to two-port MIMO and incorporate Defected Ground Structure.

The single element extended to MIMO and to create one more band, an inverted-L shaped DGS is created as shown in Figures 2(d) and 2(e). The physical attributes of the DGS are mentioned in Table 1. The resulting MIMO antenna operates

at 3.6 GHz, 4.47 GHz, and 5.53 GHz with S11 values of -20.23 dB, -16.92 dB, and -34.34 dB. The Stripline structure at the top of the patch is tuned to get the proper bandwidth for the WiMAX, 5GHz Wi-Fi, and Advanced 5G applications.

Table 1. Stage-wise dimensions and performance parameters of the proposed antenna

Stages	Antenna Dimensions (in mm)	Antenna Performance Parameters	
		Parameter	Value
Stage1: Square MSPA with Partial Ground	L_p=10, W_p=10, L_{sub}=30, W_{sub}=20, L_f=14, W_f=2, L_g=10.3, W_g=20	Centre frequency (GHz)	4.58
		S11 (dB)	-34.66
		BW (GHz)	2.55 (3.47 to 6.02)
		Gain (dBi)	2.5
		Impedance(ohms)	1.0194 + 0.0319i
Stage2: Patch loaded with CSRR and Square loop strip line.	R_1=2.22, R_2=4.285, g=0.78, L_{sa}=2.4, L_{sb}=1.8, L_{sc}=2.2, L_{sd}=0.8, W=0.2	Centre frequency (GHz)	3.89, 4.9
		S11 (dB)	-28.25, -22.71
		BW (GHz)	1.4 (3.08 to 4.48), 1.85(4.69 to 6.54)
		Gain (dBi)	2.66
		Impedance(ohms)	1.1022 + 0.4753i, 1.1315 + 0.0841i
Stage3: CSRR-loaded antenna with CPW feed	L_{cpw}=2, W_{cpw}=8, S=1	Centre frequency (GHz)	4.1, 5
		S11 (dB)	-41.42, -22
		BW (GHz)	1.4 (3.07 to 4.47), 4.13 (4.75 to 8.88)
		Gain (dBi)	2.7
		Impedance(ohms)	0.9982 + 0.0169i, 1.1313 + 0.1290i
Stage4: Two-port MIMO with Inverted L-shaped DGS	L_{MIMO}=63, W_{MIMO}=20, L_{DA}=6.3, L_{DB}=1, L_{DC}=1.7, L_{DD}=3.2, L_{DE}=8, L_{DF}=2.2	Centre frequency (GHz)	3.6, 4.47, 5.53
		S11 (dB)	-20.23, -16.92, -34.34
		S21 (dB)	>-25
		BW (GHz)	1.41 (2.65 to 4.06), 0.58 (4.34 to 4.92) 1.84 (5.16 to 7)
		Gain (dBi)	3.1
		Impedance(ohms)	1.0656 + 0.1911i, 1.2574 + 0.1949i, 0.9820 – 0.0335i

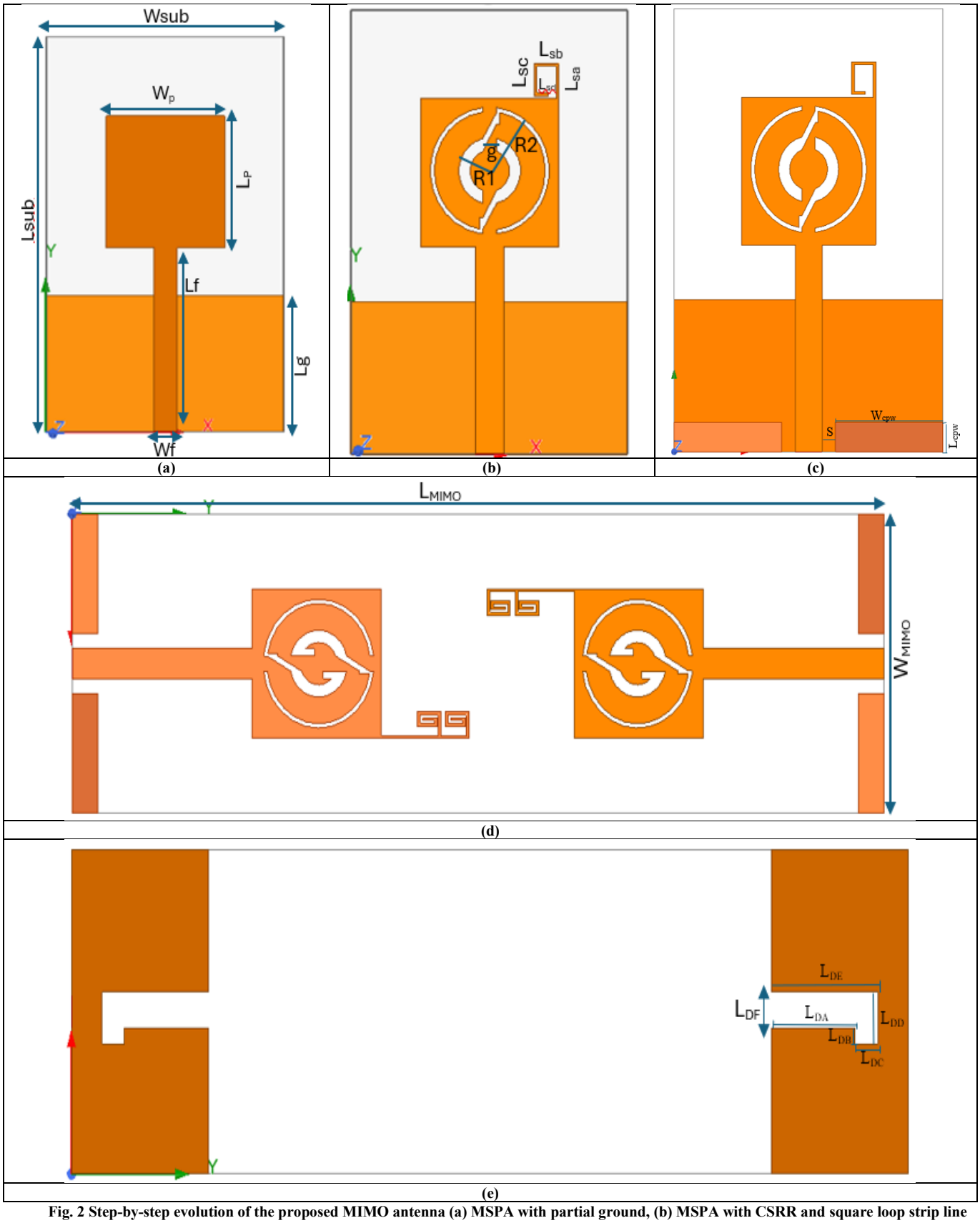

(a) (b) (c)

(d)

(e)

Fig. 2 Step-by-step evolution of the proposed MIMO antenna (a) MSPA with partial ground, (b) MSPA with CSRR and square loop strip line (c) CSRR MSPA with CPW feed, (d) MIMO (front view), and (e) MIMO (back view).

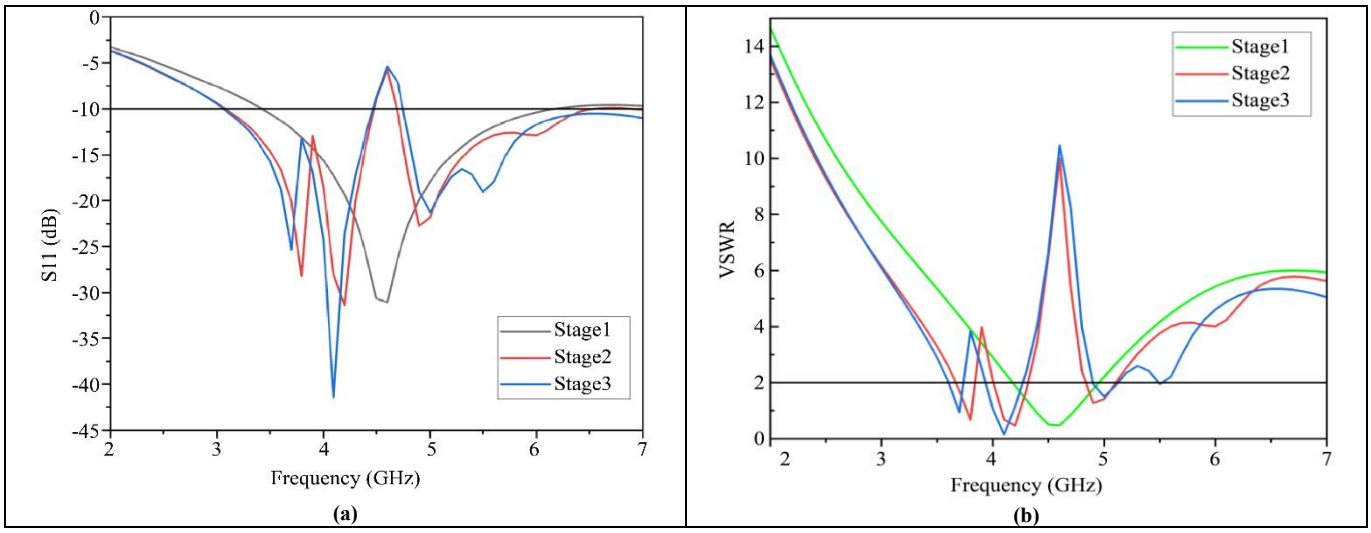

Fig. 3 (a) S11 vs Frequency of first three stages, and (b) VSWR vs frequency of first three stages.

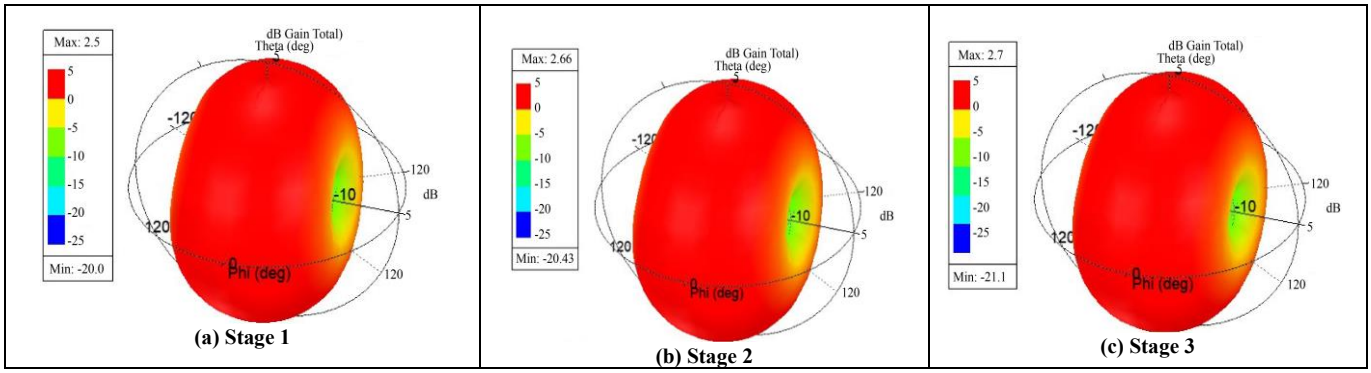

Fig. 4 Gain plots

4. Performance Analysis of the Designed MIMO Antenna

The appropriateness of the designed MIMO antenna to any application can be assessed using the parameters such as Isolation, Correlation among antennas, DG, TARC, and CCL.

4.1. Return Loss (S11) and Isolation (S21)

Return loss signifies the effective delivery of power to the antenna from the source. Typically, the S11 should be less than -10 dB for an ideal case. The higher the value of S11, the better the impedance matching, which in turn shows excellent radiation efficiency. The designed antenna shows S11 well below -17 dB for all the bands, as in Figure 5. S11 below -17dB signifies that 98% percent of input power has been radiated with minimal reflection. This also shows the efficient utilization of power by the antenna that improves the overall link budget. The isolation in MIMO implies the electromagnetic separation between the two antennas. The S21 should be less than -20 dB in MIMO. The S21 results in Figure 5 show the isolation of less than -23dB for all the bands. Isolation less than -23 dB exhibits superior performance to maintain independent paths for the MIMO signals. A better value of isolation minimizes the ECC, which is responsible for the enhancement of spatial diversity and channel capacity. Excellent isolation avoids the need for additional filtering components in the RF Front end, which reduces the cost and space. These values of S11 and S21 result in an efficient communication link, which is very much necessary in indoor and densely populated areas.

4.2. Envelope Correlation Coefficient (ECC)

ECC signifies how antennas operate independently in a wireless environment. The lesser the value of ECC, the better the diversity, indicating that the correlation between the signals from different antennas is less. The maximum limit for ECC is 0.5. Equation (2) mathematically describes the ECC of the MIMO. The ECC for the designed antenna is ≤0.006 for the plain ground and ≤0.0375 for the ground with L-shaped DGS, as indicated in Figure 6. The achieved value of ECC demonstrates its excellent diversity performance by exploiting multipath propagation, which improves data throughput. Practically, in urban, indoor, and densely populated areas, the MIMO antenna with this characteristic promises a stable signal with reduced interference. This shows the antenna is very suitable for 5G and IoT applications, which demand superior link quality and diversity performance.

$$ECC = \frac{(|S_{11}*S_{12}*S_{21}*S_{22}|)^2}{(1-|S_{11}{}^2|-|S_{21}{}^2|)(1-|S_{22}{}^2|-|S_{12}{}^2|)} \quad (2)$$

$$DG = 10\sqrt{1-ECC^2} \quad (3)$$

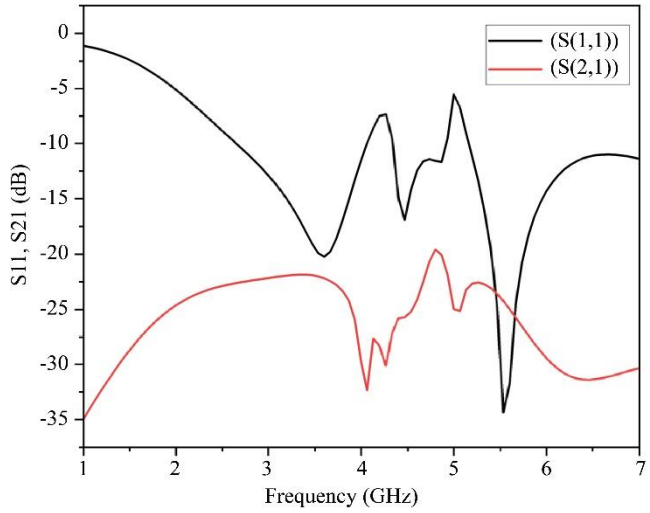

Fig. 5 Return Loss (S11) and Isolation (S21)

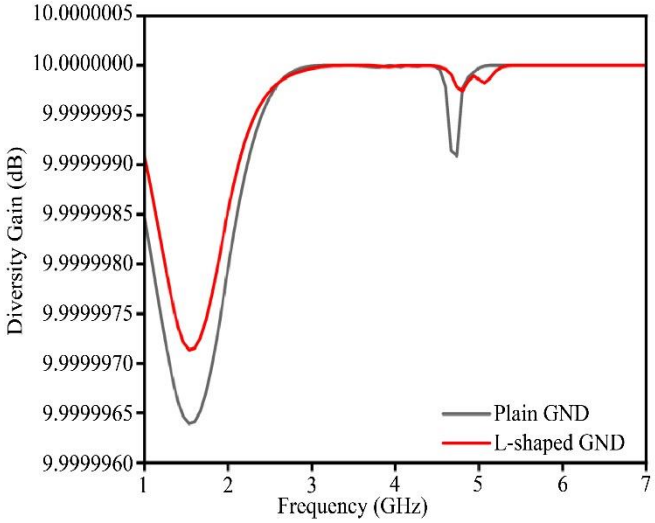

Fig. 7 Diversity Gain vs Frequency

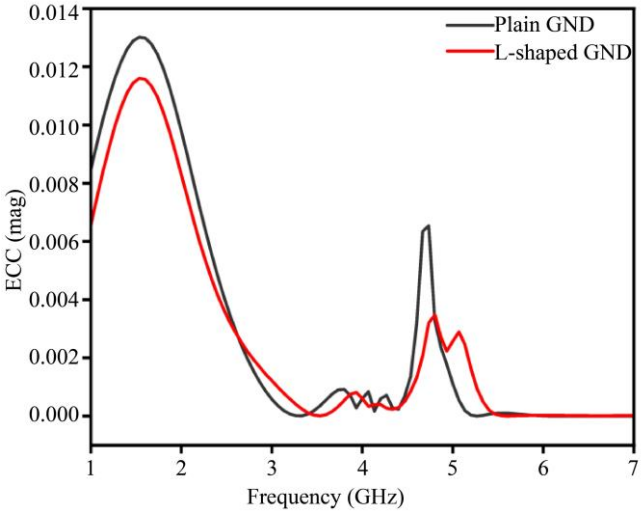

Fig. 6 ECC vs Frequency

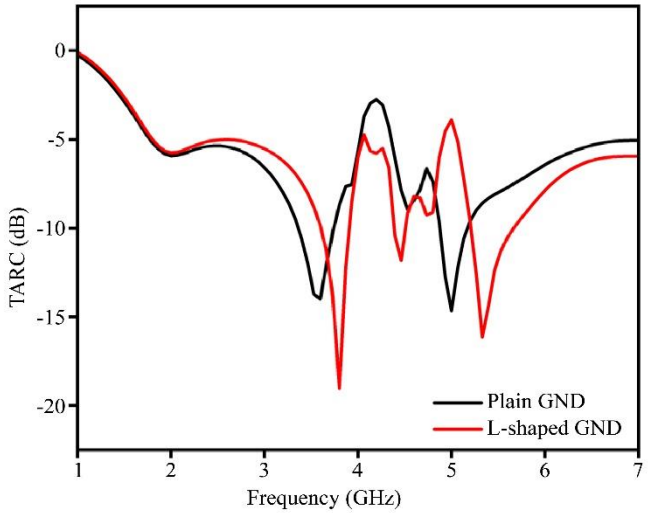

Fig. 8 TARC vs Frequency

4.3. Diversity Gain (DG)

The capability of the MIMO antennas to receive the same signal from multiple paths to improve the signal reliability or quality can be described as Diversity Gain. The value of DG should be almost ≥9.99 for a better performance. The DG becomes crucial in the indoor and urban areas where reflection and obstruction of the signal are common. The DG mainly depends on the value of ECC by the relation given by Equation (3). The designed MIMO antenna gives a DG of 9.99995 ≈10 for all the operating bands of MIMO. Figure 7 plots the DG vs frequency characteristics of the implemented MIMO antenna with and without DGS. The value 9.99995 dB for a diversity gain signifies the performance is close to an ideal MIMO antenna. This value demonstrates the antenna's ability to perform well under varying environmental conditions by mitigating multipath fading, particularly in dense urban and indoor wireless environments.

4.4. Total Active Reflection Coefficient (TARC)

TARC is the parameter that measures radiated power over reflected power, particularly in the MIMO antennas when all the antennas are excited at the same time. To optimize the signal loss, the TARC parameter will be considered. The typical value of TARC for a MIMO should be less than -10 dB, which dictates excellent matching in impedance and minimum reflections. The designed MIMO exhibits a TARC value of less than -10dB for plain ground and DGS, as in Figure 8. The TARC value is mathematically described by Equation (4) for two-port MIMO. The obtained value of TARC confirms significant power radiation when multiple ports are excited simultaneously. This implies the antenna radiates most of the fed power without significant losses. In wireless environments, particularly where multi-path is prominent, less than -10 dB of TARC contributes to enhanced data throughput and link stability.

$$TARC = \frac{\sqrt{(S_{11}+S_{22})^2+(S_{21}+S_{22})^2}}{\sqrt{2}} \quad (4)$$

4.5. Channel Capacity Loss (CCL)

The depletion in the data throughput in a MIMO refers to the CCL. The too close spacing of antenna elements, reduction in the number of independent paths due to a lack of much scattering in the environment, results in a decrease in the rank of the channel matrix and thus affects the data rate. The S-parameters S11 and S12 relate to the CCL as mentioned in Equation (5). In practical applications, such as 5GHz Wi-Fi and Advanced 5G CCL < 0.5 is considered for better performance. The designed MIMO antenna shows better CCL values (<0.175 bits/sec/Hz) for each operating band (2.65 GHz to 4.06 GHz, 4.34 GHz to 4.92 GHz, 5.16 GHz to 7GHz) plotted in Figure 9 and ensures excellent performance.

$$CCL = -log_2(1 - |S_{11}^2| - |S_{12}^2|) \quad (5)$$

The value 0.175 bits/s/Hz implies that correlation and mutual coupling effects are well controlled to permit each port to operate independently towards data transmission. In real-time scenarios, such characteristics result in excellent performance under various environments (Urban, Dense, Indoor). Hence, the antenna is very suitable for advanced 5G sub-6 GHz applications.

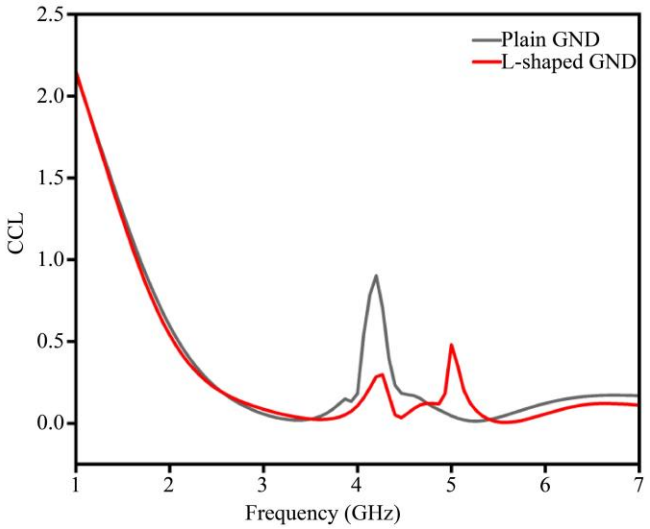

Fig. 9 CCL versus Frequency

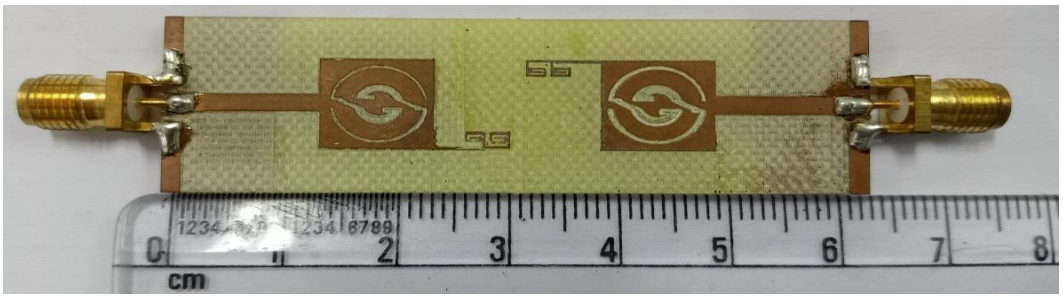

Fig. 10 Fabricated Antenna- Front view

Fig. 11 Fabricated antenna -back view

5. Measurement and Comparison

The antenna is printed over a FR4 substrate (εr =4.4) and has a height of 1.6mm, as illustrated in Figures 10 and 11. VNA from Keysight Technologies (E5063A) is used to measure the reflection coefficient (S11), VSWR, and isolation (S21) of the designed MIMO antenna. The simulated and measured results are in better agreement except for a minute shift in the frequency. The measured results show a good return loss of less than -40 dB for band 1, -18 dB for middles, and -22 dB for the last band. Excellent isolation (<-25 dB, <-20dB, and <-35 dB) was obtained for the respective frequency bands at 3.6 GHz, 4.47 GHz, and 5.53 GHz. The return loss of -40 dB and an isolation of -25 dB at 3.6 GHz demonstrates excellent impedance matching and optimal performance well-suited for the antenna for WiMAX applications that require high data rate and reliable connectivity. The S11, S21 results at 4.47 GHz imply antenna supports enhanced broadband and low latency that is essential for dense, urban, and indoor environments where multi-path fading is prominent. The values at 5.53 GHz dictate that the antenna also supports high-speed wireless LAN applications (IEEE 802.11 ac/ax). VSWR value of less than 2 can be found for all three frequency bands.

Figures 12, 13, and 14 demonstrate the S11, VSWR, and S21 versus frequency graphs of the fabricated antenna measured using VNA. There is little shift in the frequency due to the fabrication, such as variations in the PCB etching (inaccuracies in very small dimensions) that lead to variations in the electrical length, parasitic effects introduced by the manual soldering of SMA connectors (misalignment of connectors and inconsistent soldering), etc. Table 2 illustrates the comparison of the designed with existing MIMO antennas.

The compact antenna with a dimension of 63*20 mm^2 indicates that it is very suitable for embedded or portable WiMAX, high-speed Wi-Fi in compact devices without compromising the isolation and impedance matching.

5.1. Practical Implications of the Measured MIMO Parameters

- The S11 values below -40dB, -18dB, and -22 dB demonstrate a superior impedance matching that signifies excellent power transmission with minimal reflection across all the operating frequency bands.
- The S21 values below -25 dB, -20 dB, and -35 dB show close to ideal port isolation, providing independent signal paths by minimizing mutual coupling.
- Due to very minimal interference between the antenna elements, MIMO performance in terms of stable data throughput and higher channel capacity is achieved in environments where multi-path fading plays a prominent role.

Table 2. Analytical comparison of the proposed MIMO design with existing work

Ref.	No.of Elements	Technique	Substrate	Frequency Bands (GHz)	Gain (dBi)	Isolation (dB)	ECC	CCL	Size (mm^2)
[1]	2	Metasurface reflector	Rogers 5880 (2.2)	3.27, 4.78	7.75, 5.6	>25	0.01	-	23 * 30
[2]	2	CSRR on ground.	Rogers RT5880 (2.2)	35.3, 24.5	-	>25	0.0005	0.315	15 * 15
[3]	2	NB-SRR and Hexagonal Ring resonators	FR4 (4.4)	3.25, 6.05	5	>25	0.012	0.10	47.4*31.7
[4]	2	Pentagonal radiator with circular slot	Rogers RT5880 (2.2)	10.36, 20.43	-	>30	0.005	0.3	51*33
[7]	2	Parasitic elements and a half-circular SRR	FR4 (4.4)	3-5	-	>28	0.0000495	0.017	50*30
[10]	2	Slots and DGS	FR4 (4.4)	1.94-6.28	6.57	>30	0.003	-	35*70
[12]	2	Polarisation Diversity	Rogers RT5880 (2.2)	2.37, 3.62, 5.65	-	>18	0.01	0.29	34*32.5
[15]	2	Spider Fractal on the patch and DGS	FR4 (4.4)	2.43, 3.83, 4.4, 5.8	2	>12	0.08	-	37*56
[18]	2	Slots and inverted-L with the ohm symbol	FR4 (4.4)	2.2,4.1, 5.5, 5.9, 9.1	>3.5	>20	-	0.38	85*40
[This Work]	2	CSRR, Square loop strip line, and DGS	FR4 (4.4)	3.6, 4.47, 5.53	3.1	>23	0.006	0.175	63*20

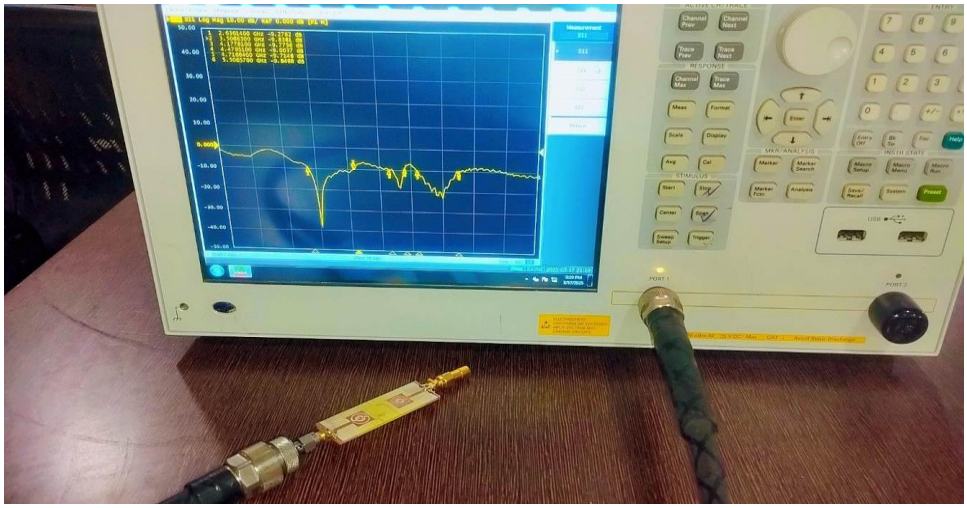

Fig. 12 Measured S11 results

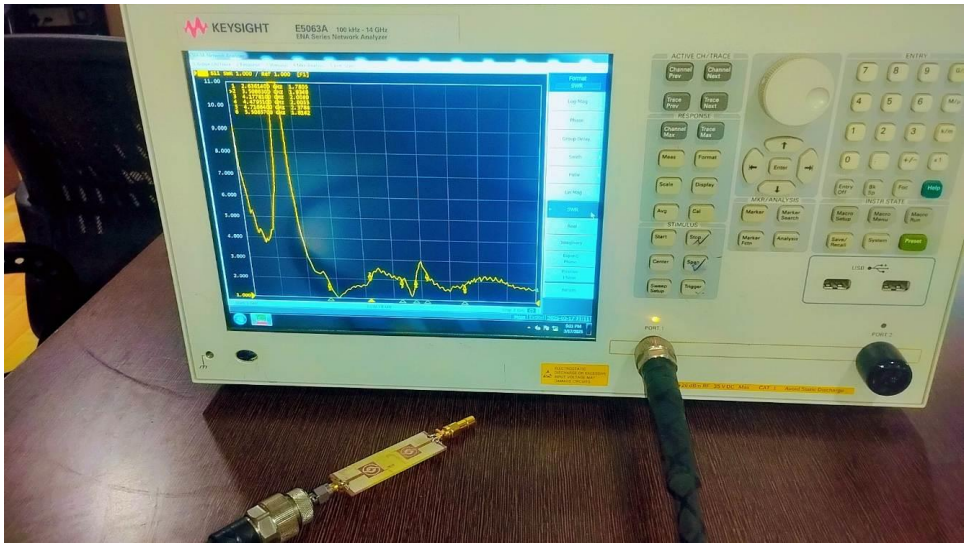

Fig. 13 Measured results of VSWR

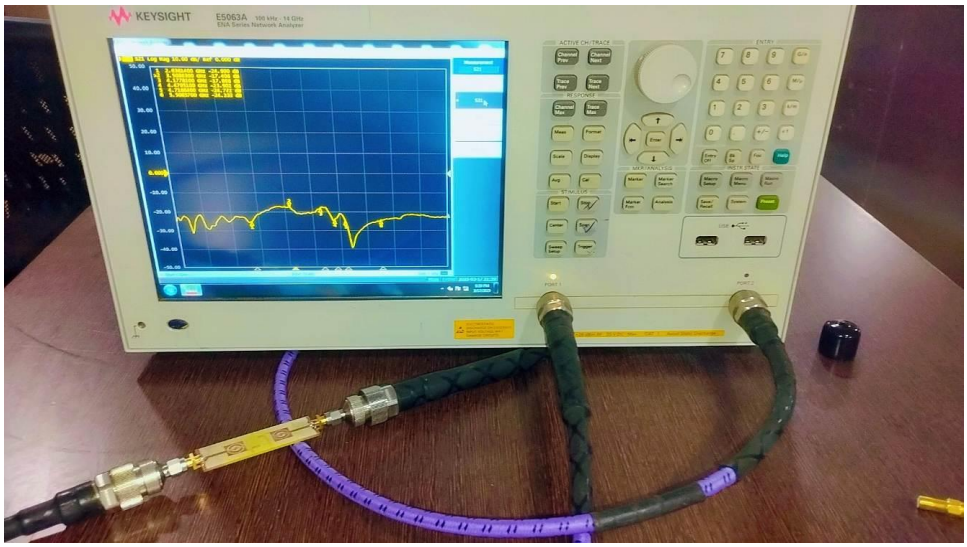

Fig. 14 Measured S21 results

6. Conclusion

A MIMO antenna with two elements for multi-band operation is designed using the combination of CSRR, CPW feed, and DGS, and discussed. The evolution of the antenna results shows that CSRR on the radiating patch resulted in a dual-band from the wide band by improving the gain.

The Square loop strip lines were used to improve the S11 and impedance bandwidth. Furthermore, the inverted-L-shaped DGS yields a multi-band characteristic. Conventionally, the tuning of square loop strip lines, dimensions of the CSRR, and DGS resulted in a multi-band MIMO operating in the sub-6GHz band with very good performance parameters. The developed antenna works at 3.6 GHz, 4.47 GHz, and 5.53 GHz with a bandwidth of 1.14 GHz, 0.58 GHz, and 1.8 GHz. S11, VSWR, and S21 are experimentally measured using a VNA setup. The measured parameters are in good agreement with the simulated. A small shift in the frequency observed due to minute variations in fabrication. The designed MIMO antenna provides a return loss < -17dB, Isolation < -20dB, ECC<0.006, DG>9.995, and CCL< 0.175 bits/sec/Hz. Hence, the observed diversity and impedance parameters show the impact of the designed antenna in the 5G sub-6GHz applications, specifically in 5GHz Wi-Fi, WiMAX, and Advanced 5G applications. Further, the antenna design can be enhanced by incorporating additional elements to improve the gain and adopting machine learning techniques. The impact of the substrate on the MIMO parameters can also be studied by choosing different dielectric constant values with variations in thickness and by employing multiple feeding techniques. Also, reconfigurability can be achieved by employing PIN diodes in MIMO to be applicable for beam steering, frequency hopping, biomedical, automotive radar, and multi-standard connectivity.

References

[1] Suresh Angadi et al., "A Metasurface based Close-Proximity Two-Port Circularly Polarized MIMO Antenna for Mid-Band Sub-6 GHz 5G Applications," *AEU-International Journal of Electronics and Communications*, vol. 183, 2024. [CrossRef] [Google Scholar] [Publisher Link]

[2] N.K. Anushkannan et al., "CSRR Backed Compact Two-Port, Dual-Band MIMO Antenna for Mm-Wave Applications," *Wireless Networks*, vol. 30, no. 3, pp. 1857-1867, 2024. [CrossRef] [Google Scholar] [Publisher Link]

[3] Yugender Mood, and R. Pandeeswari, "A Novel SRR Metamaterial Inspired CPW-Fed Dual Band MIMO Antenna for Sub-6 GHz 5G Application," *Wireless Personal Communications*, vol. 130, no. 2, pp. 1277-1293, 2023. [CrossRef] [Google Scholar] [Publisher Link]

[4] Lovish Matta, Manish Sharma, and Rana Gill, "A 2×2 Multiband MIMO Antenna in the Shape of a Pentagonal Hut for X-band and K-band Applications," *2023 IEEE Renewable Energy and Sustainable E-Mobility Conference (RESEM)*, Bhopal, India, pp. 1-6, 2023. [CrossRef] [Google Scholar] [Publisher Link]

[5] Mohammad Alibakhshikenari et al., "An Innovative Antenna Array with High Inter Element Isolation for Sub-6 GHz 5G MIMO Communication Systems," *Scientific Reports*, vol. 12, no. 1, pp. 1-13, 2022. [CrossRef] [Google Scholar] [Publisher Link]

[6] Surentiran Padmanathan et al., "Compact Multiband Reconfigurable MIMO Antenna for Sub- 6GHz 5G Mobile Terminal," *IEEE Access*, vol. 10, pp. 60241-60252, 2022. [CrossRef] [Google Scholar] [Publisher Link]

[7] K. Vasu Babu et al., "Design and Development of Miniaturized MIMO Antenna using Parasitic Elements and Machine Learning (ML) Technique for Lower sub 6 GHz 5G Applications," *AEU - International Journal of Electronics and Communications*, vol. 153, 2022. [CrossRef] [Google Scholar] [Publisher Link]

[8] Ashfaq Ahmad, Dong-you Choi, and Sadiq Ullah, "A Compact Two Elements MIMO Antenna for 5G Communication," *Scientific Reports*, vol. 12, no. 1, pp. 1-8, 2022. [CrossRef] [Google Scholar] [Publisher Link]

[9] H.V. Pallavi, A.P. Jagadeesh Chandra, and Paramesha, "Design and Performance Analysis of MIMO Patch Antenna Using Superstrate for Minimization of Mutual Coupling," *WSEAS Transactions on Circuits and Systems*, vol. 21, pp. 142-153, 2022. [CrossRef] [Google Scholar] [Publisher Link]

[10] Manish Sharma, Rajesh Kumar Kaushal, and Naveen Kumar, "Two-Port MIMO Antenna with Circular Slotted Patch Designed for Bluetooth, WiMAX and WLAN Multiband Applications," *2022 8th International Conference on Signal Processing and Communication (ICSC)*, Noida, India, pp. 205-210, 2022. [CrossRef] [Google Scholar] [Publisher Link]

[11] Swarna Jayakumar et al., "Two Port MIMO Antenna for Wideband Applications," *2022 IEEE Microwaves, Antennas, and Propagation Conference (MAPCON)*, Bangalore, India, pp. 774-779, 2022. [CrossRef] [Google Scholar] [Publisher Link]

[12] Benghanem Yahia, Mansoul Ali, and Mouffok Lila, "Compact Tri-Band Two-Element MIMO Slot Antenna for 5G Sub-6 GHz Frequency Bands," *2022 2nd International Conference on Advanced Electrical Engineering (ICAEE)*, Constantine, Algeria, vol. 16, pp. 1-6, 2022. [CrossRef] [Google Scholar] [Publisher Link]

[13] P. Jeyakumar, P. Muthuchidambaranathan, and S. Shrinidhi, "A Novel Two Port High Isolation Dual-Polarized Multiband Sub-6 GHz MIMO Antenna for IoT Connected Devices," *Wireless Personal Communications*, vol. 121, pp. 2569-2587, 2021. [CrossRef] [Google Scholar] [Publisher Link]

[14] Juhi Wani et al., "Design and Fabrication of a Multi-Band 2Element MIMO Antenna for Sub-6 GHz Applications," *2021 IEEE Indian Conference on Antennas and Propagation (InCAP)*, Jaipur, Rajasthan, India, pp. 198-200, 2021. [CrossRef] [Google Scholar] [Publisher Link]

[15] Sanjay Chouhan et al., "Spider-Shaped Fractal MIMO Antenna for WLAN/WiMAX/Wi-Fi/Bluetooth/C-band Applications," *AEU-International Journal of Electronics and Communications*, vol. 110, 2019. [CrossRef] [Google Scholar] [Publisher Link]

[16] Deepika Sipal, Mahesh P. Abegaonkar, and Shiban K. Koul, "Highly Isolated Compact Planar Dual-Band Antenna with Polarization/Pattern Diversity Characteristics for MIMO Terminals," *IEEE Antennas and Wireless Propagation Letters*, vol. 18, no. 4, pp. 762-766, 2019. [CrossRef] [Google Scholar] [Publisher Link]

[17] Hesam Ekrami, and Shahrokh Jam, "A Compact Triple-Band Dual-Element MIMO Antenna with High Port-to-Port Isolation for Wireless Applications," *AEU-International Journal of Electronics and Communications*, vol. 96, pp. 219-227, 2018 [CrossRef] [Google Scholar] [Publisher Link]

[18] K. Vasu Babu, and B. Anuradha, "Design of Inverted L-shape & ohm Symbol Inserted MIMO Antenna to Reduce the Mutual Coupling," *AEU-International Journal of Electronics and Communications*, vol. 105, pp. 42-53, 2019. [CrossRef] [Google Scholar] [Publisher Link]

[19] Ziyang Wang, Chenglei Li, and Yingzeng Yin, "A Meta-Surface Antenna Array Decoupling (MAAD) Design to Improve the Isolation Performance in a MIMO System," *IEEE Access*, vol. 8, pp. 61797-61805, 2020. [CrossRef] [Google Scholar] [Publisher Link]

[20] Zeba Parveen, and Megha Dadel, "Two Port Multi-band MIMO Antenna with FSS Implementation," *2018 International Conference on Wireless Communications, Signal Processing and Networking (WiSPNET),* Chennai, India, pp. 1-4, 2018. [CrossRef] [Google Scholar] [Publisher Link]

[21] Yingying Yang, Qingxin Chu, and Chunxu Mao, "Multiband MIMO Antenna for GSM, DCS, and LTE Indoor Applications," *IEEE Antennas and Wireless Propagation Letters*, vol. 15, pp. 1573-1576, 2016. [CrossRef] [Google Scholar] [Publisher Link]

[22] Debaprasad Barad et al., "A CSRR Loaded Triple-Band Microstrip Patch Antenna with Suppressed Higher Order Modes for Sub-6 GHz Phased Array Application," *2022 IEEE Microwaves, Antennas, and Propagation Conference (MAPCON)*, Bangalore, India, pp. 903-908, 2022. [CrossRef] [Google Scholar] [Publisher Link]

[23] Huthaifa A. Al Issa, Yahyakhr S.H. Khraisat, and Fatima A.S. Alghazo, "Bandwidth Enhancement of Microstrip Patch Antenna by Using Metamaterial," *International Journal of Interactive Mobile Technologies (iJIM)*, vol. 14, no. 1, pp. 169-175, 2020. [CrossRef] [Google Scholar] [Publisher Link]

[24] S. Nelaturi, and N.V.S.N. Sarma, "CSRR based Patch Antenna for Wi-Fi and WiMAX Applications," *Advanced Electromagnetics*, vol. 7, no. 3, pp. 40-45, 2018. [CrossRef] [Google Scholar] [Publisher Link]

[25] R. Samson Daniel, R. Pandeeswari, and S. Raghavan, "Multiband Monopole Antenna Loaded with Complementary Split Ring Resonator and C-Shaped Slots," *AEU- International Journal of Electronics and Communications*, vol. 75, pp. 8-14, 2017. [CrossRef] [Google Scholar] [Publisher Link]

[26] Varindra Kumar, "Patch Antenna Miniaturization Using CSRR," *Open Journal of Antennas and Propagation*, vol. 5, no. 3, pp. 132-150, 2017. [CrossRef] [Google Scholar] [Publisher Link]

[27] Murtala Aminu-Baba et al., "Microstrip Antenna with CSRR Ground Structure," *2017 International Symposium on Antennas and Propagation (ISAP)*, Phuket, Thailand, pp. 1-2, 2017. [CrossRef] [Google Scholar] [Publisher Link]

[28] Mehrab Ramzan, and Kagan Topall, "A Miniaturized Patch Antenna by Using a CSRR Loading Plane," *International Journal of Antennas and Propagation*, vol. 2015, pp. 1-9, 2015. [CrossRef] [Google Scholar] [Publisher Link]

[29] Aziz Dkiouak et al., "A Dual-Port MIMO Antenna System for 5G and Wi-Fi 6E Communications using a Parasitic Element," *e-Prime - Advances in Electrical Engineering, Electronics and Energy*, vol, 10, pp. 1-10, 2024. [CrossRef] [Google Scholar] [Publisher Link]

[30] Naguboina Gopi Chand, and K. Anusudha, "Compact Two-Port Dual- and Triple-Band MIMO Antennas with Orthogonally Placed Microstrip Monopole Elements for 5G N77/78/79 Sub-6-GHz Applications," *International Journal of Communication Systems*, vol. 38, no. 13, 2025. [CrossRef] [Google Scholar] [Publisher Link]

[31] Deepthi Mariam John et al., "A Dual-Band Flexible MIMO Array Antenna for Sub-6 GHz 5GCommunications," *Sensors*, vol. 25, no. 11, pp. 1-22, 2025. [CrossRef] [Google Scholar] [Publisher Link]